Supporting Information: Emissive perovskite quantum wires in robust nanocontainers: $CsPbX_3$ confined inside boron nitride nanotubes

Bea Botka,[*,†] Erzsébet Dodony,[‡] Gergely Németh,[†,¶] Michael Stratton,[†] Ildikó Harsányi,[†] János Mózer,[†,§] Éva Kováts,[†] Ferenc Borondics,[‖] and Katalin Kamarás[†,‡]

†*Institute for Solid State Physics and Optics, HUN-REN Wigner Research Centre for Physics, Budapest, 1121, Hungary*

‡*Institute for Technical Physics and Materials Science, HUN-REN Centre for Energy Research, Budapest, 1121, Hungary*

¶*SOLEIL Synchrotron, Saint Aubin 91190, France*

§*Faculty of Natural Sciences, Budapest University of Technology and Economics, Hungary*

‖*SOLEIL Synchrotron, Saint Aubin, 91190, France*

E-mail: botka.bea@wigner.hun-ren.hu

The supporting information contains additional data on the starting perovskite materials and potential processing byproducts, mixed halide nanowires confined in BNNTs, $CsPbBr_3$ in SWCNTs and embedded in hBN. EDS analysis, temperature-dependent photoluminescence spectra of the different BNNT-confined structures and polarization PL image series of $CsPbX_3$@BNNT, and an external $CsPbBr_3$ particle are also included.

Contents

1 Additional STEM and EDS data

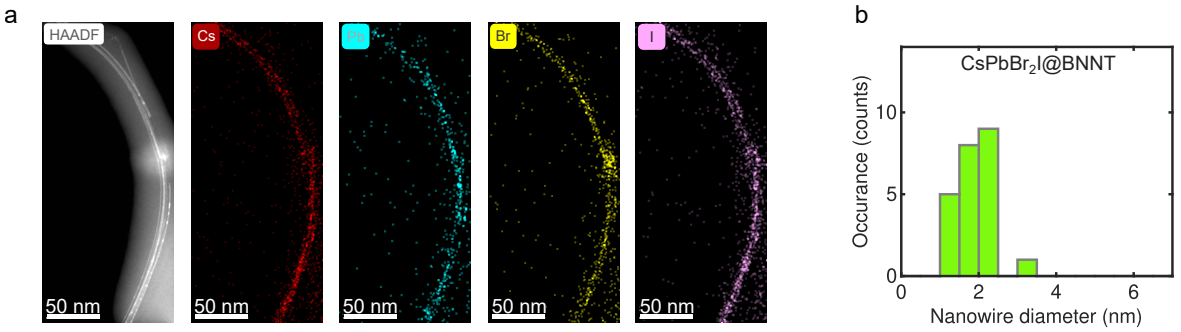

Figure S1: (a) High-angle annular dark field scanning transmission electron microscopy image of $CsPbBr_2I$@BNNT and elemental maps. (b) Diameter distribution of the nanowires based on a larger number of HAADF STEM images.

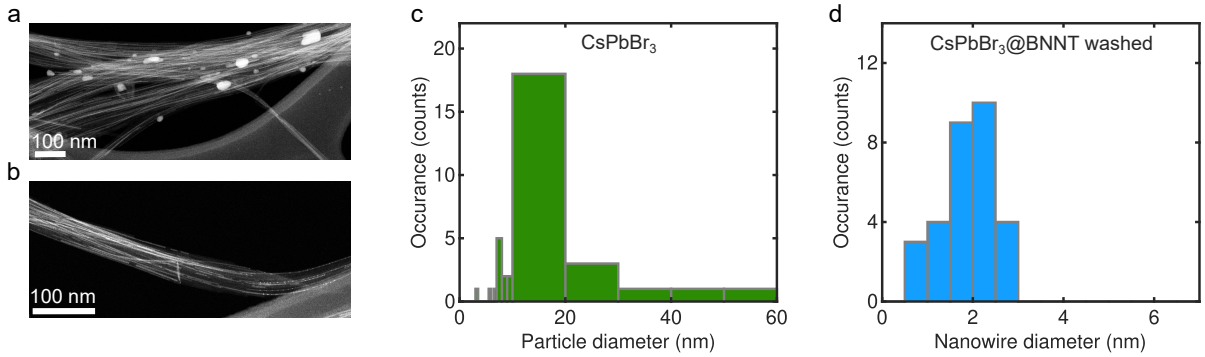

Figure S2: High-angle annular dark field scanning transmission electron microscopy images of $CsPbBr_3$@BNNT samples (a) before and (b) after DMF washing. Diameter distribution of (c) the non-encapsulated perovskite nanoparticles present before washing and (d) nanowires in the washed sample. Histograms were created based on a larger set of HAADF STEM images.

EDS was performed in STEM and TEM mode. Data presented in Tables S1-S3 were recorded on larger bundle sections. It is typical for few unit cell wide wires that the Cs and Br/I ratio is higher than in the bulk material. To estimate the filling efficiency between various samples, the number of Pb to (B+N) atoms were used in addition to the TEM images. As a reference, the most abundantly observed nanowires, the 2x2 and 3x3 unit cell perovskites, in a 3-walled BNNT at 100% filling rate would correspond to $6*10^{-3}$ and $11*10^{-3}$ Pb to

(B+N) ratio, respectively. The BNNTs consist of dominantly 3 or 4 walls.

Table S1: Elemental composition from the EDS recorded on the $CsPbBr_3$@BNNT sample. The sample was not washed, but EDS analysis was performed on sections where no adsorbed particles were present.

Element	Family	Atomic Fraction (%)	Atomic Error (%)
B	K	53.45	4.72
N	K	44.00	4.94
Br	K	1.49	0.23
Cs	L	0.69	0.1
Pb	L	0.37	0.05

Table S2: Elemental composition from the EDS recorded on the DMF-washed $CsPbBr_3$@BNNT sample.

Element	Family	Atomic Fraction (%)	Atomic Error (%)
B	K	52.74	4.77
N	K	45.20	4.96
Br	K	1.29	0.20
Cs	L	0.47	0.07
Pb	L	0.30	0.04

Table S3: Elemental composition from the EDS recorded on the $CsPbI_3$@BNNT sample. The sample was not washed, but EDS analysis was performed on sections where no adsorbed particles were present.

Element	Family	Atomic Fraction (%)	Atomic Error (%)
B	K	53.88	4.63
N	K	42.90	4.90
I	K	1.83	0.25
Cs	L	0.75	0.10
Pb	L	0.64	0.09

Table S4: Elemental composition from the EDS recorded on the $CsPbBr_2I$@BNNT sample, based on the elemental maps shown in Figure S1.

Element	Family	Atomic Fraction (%)	Atomic Error (%)
B	K	66.76	4.17
N	K	30.75	4.31
Br	K	0.92	0.13
I	L	0.55	0.07
Cs	L	0.49	0.06
Pb	L	0.52	0.07

2 Photoluminescence spectra recorded in inert atmosphere

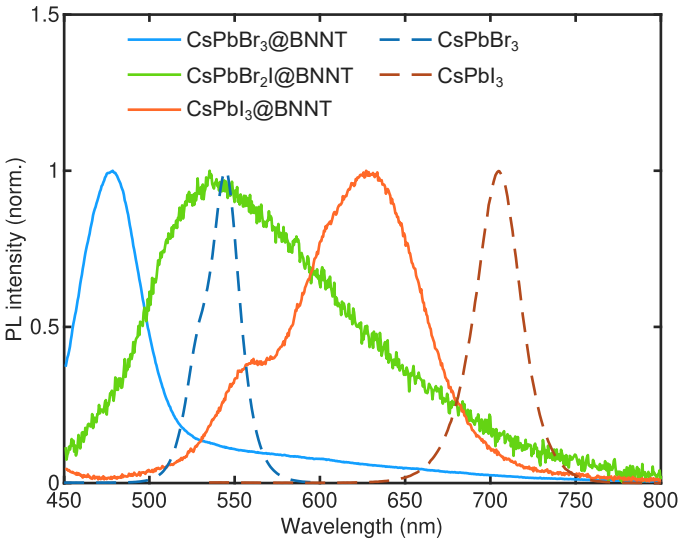

Figure S3: PL spectra of as-prepared perovskite@BNNT samples in inert atmosphere normalized to the intensity maximum. Samples used for the measurements had no exposure to ambient environment or any solvents. PL spectra were recorded inside an Ar-filled glovebox using 405 nm excitation. As a reference, spectra with dashed lines show emission of the bulk perovskite precursors used for the filling from S4c and d (recorded in air).

3 Perovskites used for BNNT filling

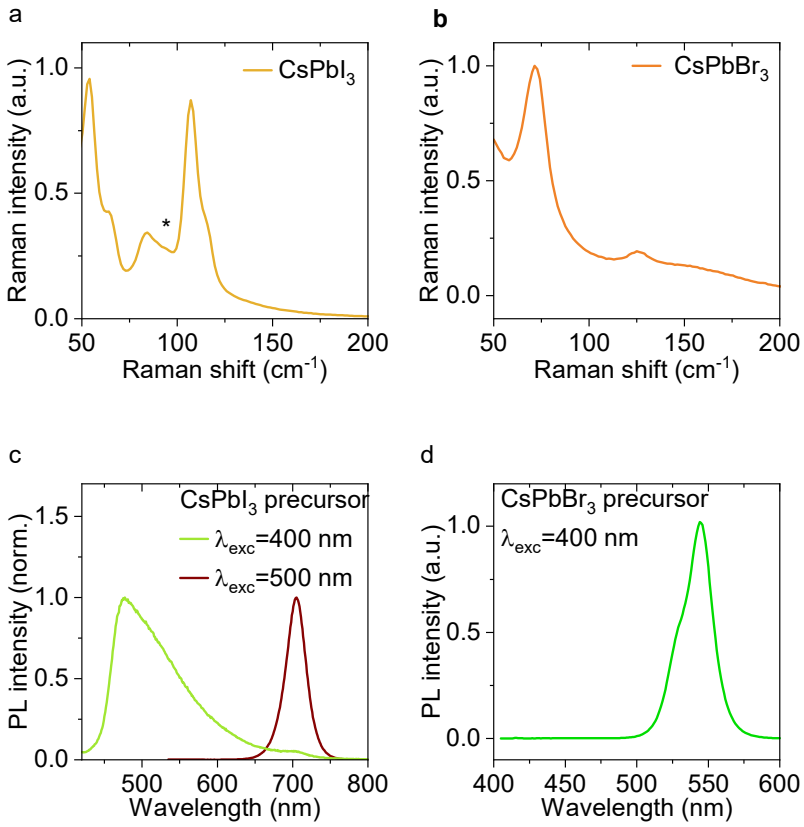

Figure S4: Raman spectra of the non-encapsulated precursor residues remaining in the bottom of the quartz tubes after the synthesis of (a) $CsPbI_3$ and (b) $CsPbBr_3$ quantum wires. Photoluminescence spectra of (c) the $CsPbI_3$ and (d) $CsPbBr_3$ precursor used for the filling of the BNNTs. All spectra are normalized to the intensity maximum.

The yellow color of the $CsPbI_3$ powder used for the filling and its Raman spectrum (Figure S4a) indicate that it is dominantly crystallized in the non-emissive δ-phase.[1] Presence of the PbI_2 (also marked with * on the Raman spectrum),[1] and the γ-$CsPbI_3$ impurities in the sample can be observed on the PL spectra (Figure S4c), corresponding to the 700 nm emission observed using 500 nm excitation wavelength. $CsPbBr_3$ precursor is present in its orthorhombic phase (Figure S4b), the lower energy peak in the PL (Figure S4d) is due to the defective nature of the crystals.[2–4]

4 Reference for non-confined species

Figure S5 shows $CsPbBr_3$@BNNT samples prepared under identical conditions, but using different BNNT sources. BNNT-1 was prepared from BNNT SP10RP 11B BNNT source from BNNT LLC. The nanotubes were opened by 4 hours bath sonication in ammonium hydroxide and cleaned according to the procedure described in Ref. 5. BNNT-2 was received open-ended from BNNT LLC and used as-received for filling. BNNT-1 contains shorter tubes, and a large excess of hBN flakes covering them. (Figure S5 b,c) BNNT-1 and 2 has a similar diameter distribution, BNNT-1 being potentially marginally larger. Perovskite quantum wires can be observed in both BNNT-1 and 2, but in BNNT-1 the encapsulation was not very efficient, potentially due to the tube ends being blocked. On the other hand a significant amount of perovskite nanoparticles can be observed, entangled in the hBN network. This would offer them some protection, similar to the BNNTs, but does not have a strict upper limit for their size. The photoluminescence of $CsPbBr_3$@BNNT is centered at 514 nm, significantly redshifted compared to the $CsPbBr_3$@BNNT-2 sample, having confined quantum wires.

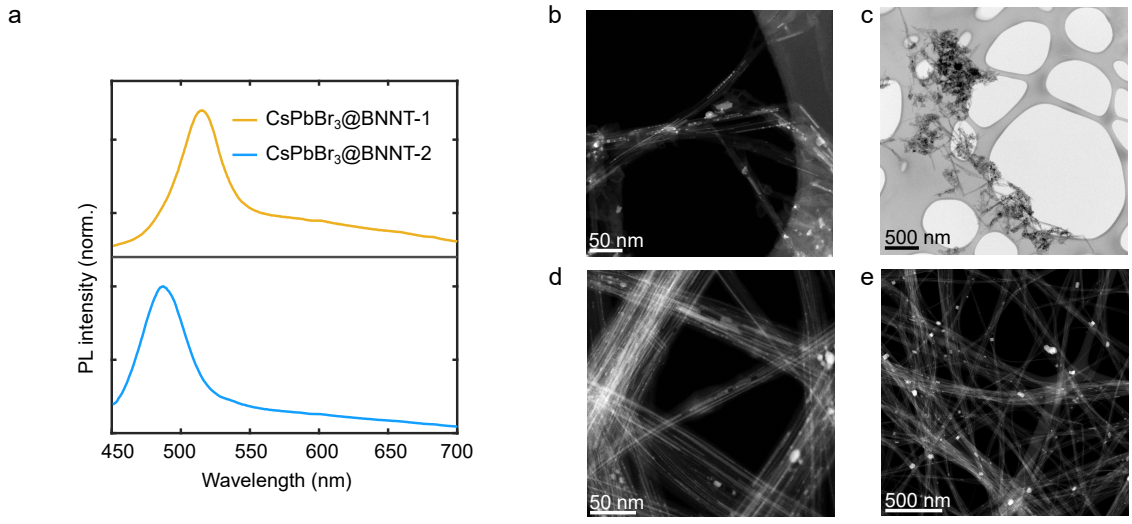

Figure S5: Comparison of samples prepared using different BNNT hosts. (a) Photoluminescence spectra of the as-prepared samples recorded inside the glovebox using 405 nm excitation wavelength, normalized to the intensity maximum. STEM HAADF and TEM images of (b,c) $CsPbBr_3$@BNNT-1 samples and (d,e) $CsPbBr_3$@BNNT-2 samples.

5 A note on formation of byproducts

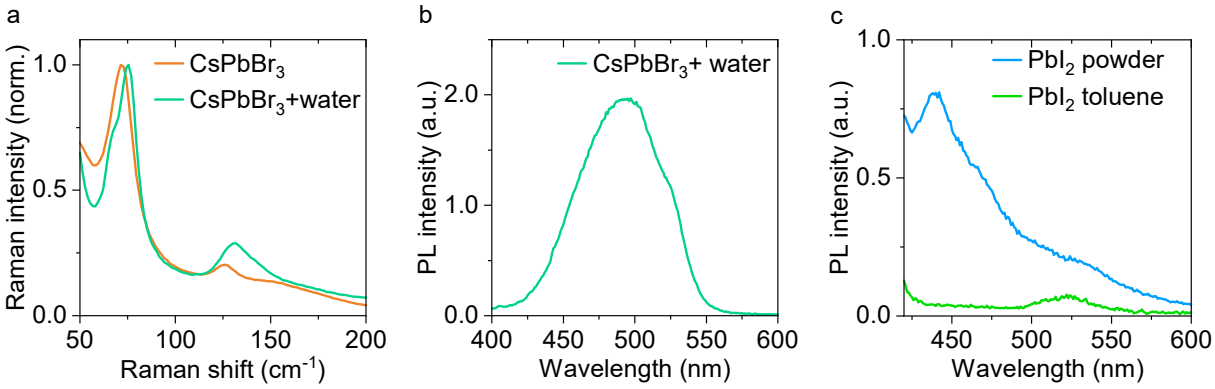

Figure S6: (a) Raman spectra of $CsPbBr_3$ powder and water vapor-treated $CsPbI_3$ on Si normalized to the intensity maximum. The newly appearing peaks after water treatment indicate the formation of $CsPb_2Br_5$.[2] (b) PL spectrum of the water-treated $CsPbBr_3$, showing emission of small $CsPbBr_3$ nanoparticles encapsulated inside the $CsPb_2Br_5$ recorded using 350 nm excitation. (c) Photoluminescence spectra of the PbI_2 in powder form and coated onto a surface from toluene solution recorded using 400 nm excitation.

In any processing or washing steps, byproducts can form outside the nanotubes, these are important to be aware of. As discussed in the main text, exposure to water (or any AX-selective solvent, such as alcohols) can result in initial passivation and PL increase of the adsorbed particles, then progressively to the formation of $CsPb_2X_5$ and CsX..[6–8] In this reaction also highly luminescent core-shell particles can form, that are particularly stable against environmental degradation (Fig. S6a,b).[9]

The non-encapsulated material is present in the form of small, unprotected nanoparticles. Their high surface to volume ratio makes their optical properties extremely sensitive to chemical changes. In case of optical measurements performed on ensembles it is often complicated to separate spectral features arising from these altered nanoparticles from those of the encapsulated species.

For $CsPbBr_3$@BNNT, the emission of the adsorbed particles falls dominantly above 500 nm based on the observed size distribution, but core-shell particles can have larger apparent sizes. For $CsPbI_3$, emission from larger γ-phase nanoparticles is expected close to

700 nm. However, iodide-based perovskites are more sensitive to water-exposure, therefore formation of PbI_2 is likely as well, resulting in new emission peak in the blue-green range depending on their size (Fig. S6c).

6 Temperature dependence of the photoluminescence

Figure S8 demonstrates the temperature dependent photoluminescence spectra recorded on $CsPbBr_3$@BNNT and $CsPbI_3$@BNNT. As reference, nanoparticles of $CsPbBr_3$ embedded in $CsPb_2Br_5$ were prepared by exposing $CsPbBr_3$ powder to water vapor until color change in the photoluminescence was observed and then drying the sample. The exact emission wavelength is hard to control this way, but the experiment demonstrates the effect of particle size on the temperature dependence of the PL in agreement with the literature.[10]

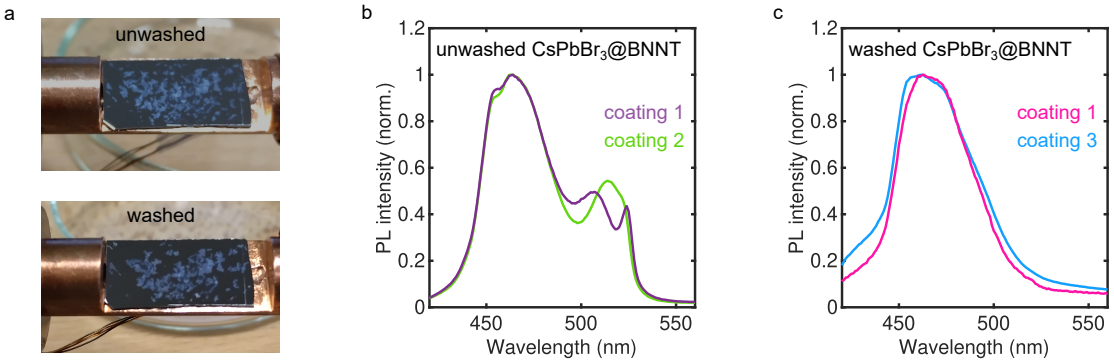

Figure S7: (a) Photos of a $CsPbBr_3$@BNNT sample before (top) and after DMF washing (bottom) show that loss of BNNTs typically occurs during washing. (b) PL spectra of unwashed $CsPbBr_3$@BNNT samples normalized to the intensity maximum. The samples were prepared as discussed in the Experimental section under Temperature dependent PL spectroscopy. Coating 1-3 refers to spin-coated samples prepared using different toluene dispersions of the same $CsPbBr_3$@BNNT sample. The distinct emission peaks above 500 nm originating from non-encapsulated perovskite nanoparticles changes between samples. (c) PL spectra of the DMF-washed samples showing reproducible emission. (Spectra are normalized to the intensity maximum.)

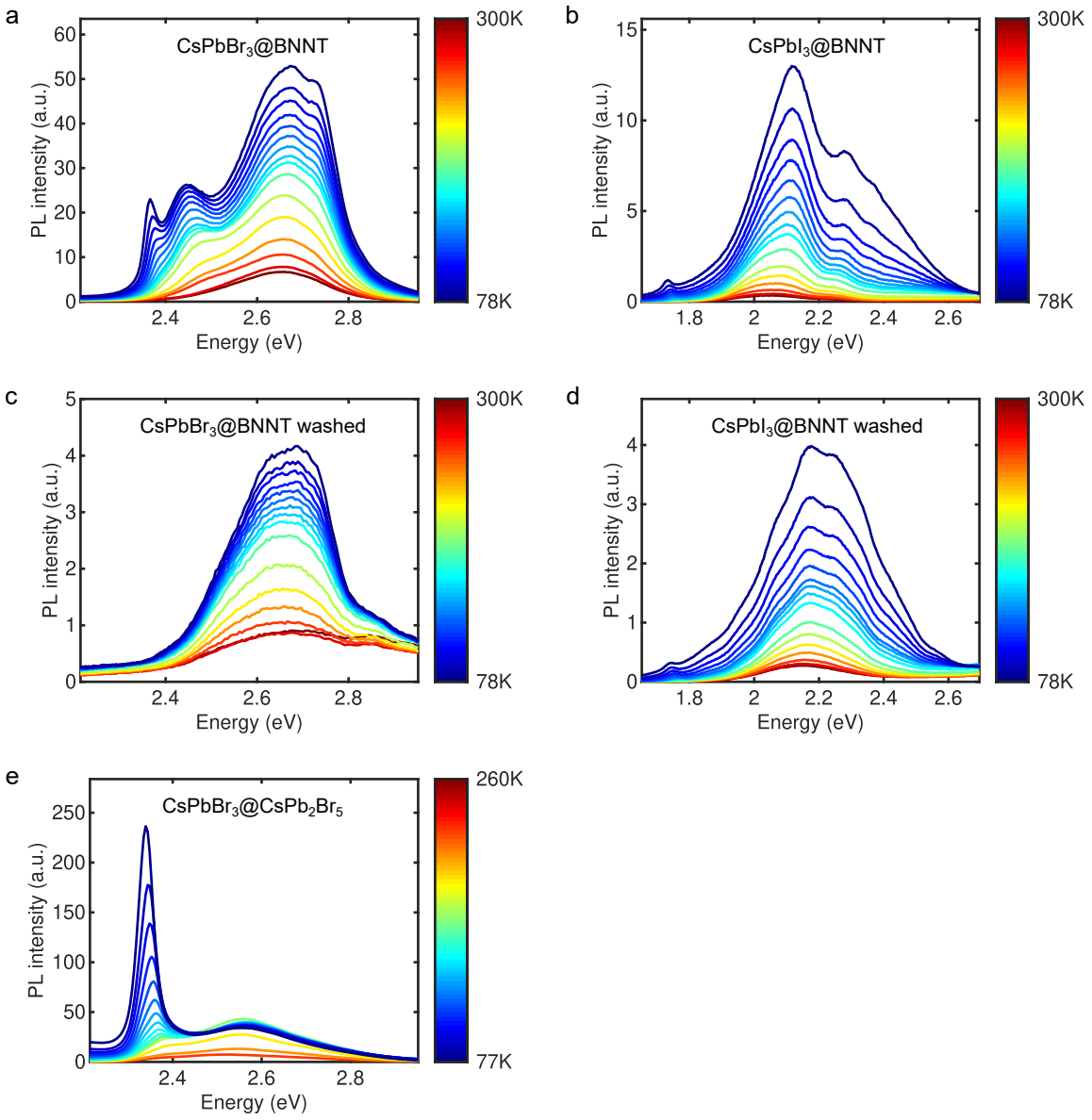

Figure S8: Photoluminescence spectra recorded on (a,c) $CsPbBr_3$@BNNT, (b,d) $CsPbI_3$@BNNT samples and (e) $CsPbBr_3$@$CsPb_2Br_5$ core-shell nanoparticles as reference at temperatures between 77 and 300 K. The unwashed samples were dispersed in toluene and spin coated without purification, the washed samples were washed with DMF several times after coating. The peaks of the non-encapsulated $CsPbBr_3$ nanoparticles are prominent in a at low temperatures (around 2.4 eV). The PL peak energies of both the bromide- and the iodide-based quantum wires show a redshift with increasing temperature, which is distinctly different from the behavior of larger non-encapsulated perovskite nanoparticles. Loss due to extended DMF washing affects more the larger diameter quantum wires.

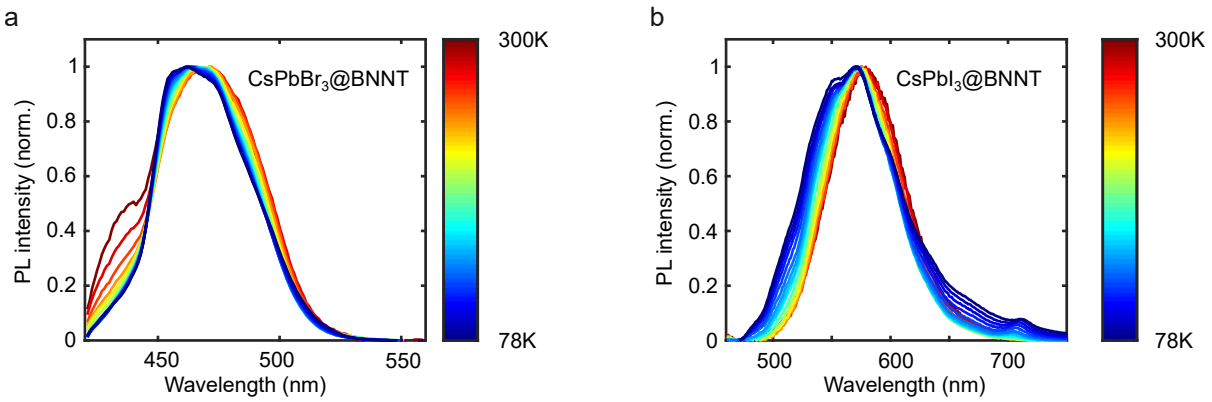

Figure S9: Photoluminescence spectra of (a) $CsPbBr_3$@BNNT and (b) $CsPbI_3$@BNNT recorded in the temperature range of 78-300 K (normalized to the intensity maximum).

7 $CsPbBr_3$@SWCNT

$CsPbBr_3$@SWCNT was prepared in a similar way as the BNNT-encapsulated ones. P2 purified electric arc synthesized single-wall carbon nanotubes with diameters 1.1-1.5 nm, were purchased from Carbon Solutions (Riverside, California). The nanotubes were opened by a 20 minute annealing at 420 °C in air. To remove functional groups the nanotubes were degassed at 100 °C for 1 hour, followed by 1 hour annealing at 800 °C in dynamic vacuum. The preprocessed SWCNT was mixed with $CsPbBr_3$ in 1:1 weight ratio inside the glovebox. The mixture was transferred into a quartz ampule and sealed under dynamic vacuum. Perovskite filling was performed at 620 °C for 12 hours, followed by annealing the mixture at 1100 °C for further 12 hours to close the nanotube ends, then cooled slowly.

The samples were stored in air after their preparation, and processed for measurements as the BNNT ones. HAADF STEM images and STEM elemental maps and EDS recorded on the $CsPbBr_3$@SWCNT demonstrate good encapsulation yield. (Fig. S10, Table S5) Change of the lineshape and shift of the G peak of the SWCNT is significantly shifted in the Raman spectra indicates charge transfer between the nanotubes and the encapsulated perovskites in agreement with earlier reports.[11] The upshift of the 2D mode can indicate p-doping,[12] but in this case strain is simultaneously present, and its contribution is potentially strongly

diameter dependent due to the differences in specific host@guest size matches. Furthermore significant change in the radial breathing mode region indicates changed resonance conditions as a result of perovskite encapsulation, further complicating the assessment. Earlier experiments performed on CsPbBr3@SWCNT field-effect transistors indicated n-doping of the host nanotubes.[11,13] At room temperature no photoluminescence was observed from the samples. At 77 K a weak emission at 524 nm was observed, which blue-shifted with increasing temperature, similar to the emission of the adsorbed perovskites. The SWCNTs used are smaller in average diameter than the BNNTs, therefore perovskite@SWCNT quantum wires are expected to have a larger bandgap. Exciton self-trapping or formation of interlayer excitons as a result of a type II heterojunction can account for redshifted emission. Therefore we also checked the behavior of the observed green emission upon washing (Figure S10e). We observed that the intensity of the green emission is strongly dependent on solvent exposure. Short exposure to DMF or long soaking in toluene in ambient atmosphere can activate the green emission (solvent-activated), but upon thorough DMF washing, similar to the one applied to the BNNTs, the emission vanished. Therefore this weak emission potentially originates from residual adsorbed nanoparticles, which might be hard to remove from within the nanotube bundles.

Table S5: Elemental composition from the EDS recorded on the $CsPbBr_3$@SWCNT sample.

Element	Family	Atomic Fraction (%)	Atomic Error (%)
C	K	95.66	0.35
Br	K	2.70	0.34
Cs	L	0.83	0.09
Pb	L	0.81	0.09

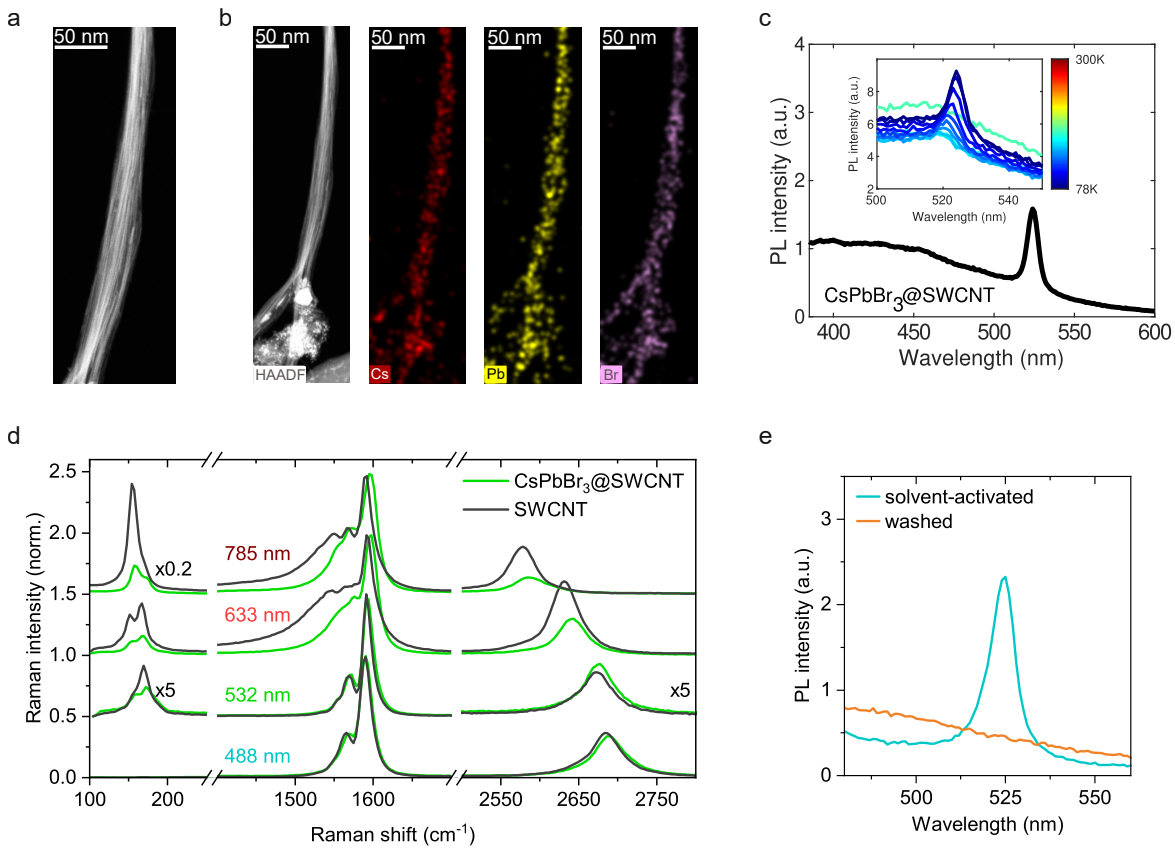

Figure S10: High-angle annular dark field scanning transmission electron microscopy image of (a) $CsPbBr_3$@SWCNT and (b) elemental maps. (c) Low temperature PL spectra of $CsPbBr_3$@SWCNT with the inset showing the temperature dependence of the emission. Excitation used for the main panel was 355 nm, for the insert 450 nm. (d) Raman spectra of the filled and reference SWCNTs at room temperature (normalized to the intensity of the G band). (e) PL spectra recorded at 78 K of a $CsPbI_3$ sample during washing steps using 400 nm excitation.

8 Polarization image series

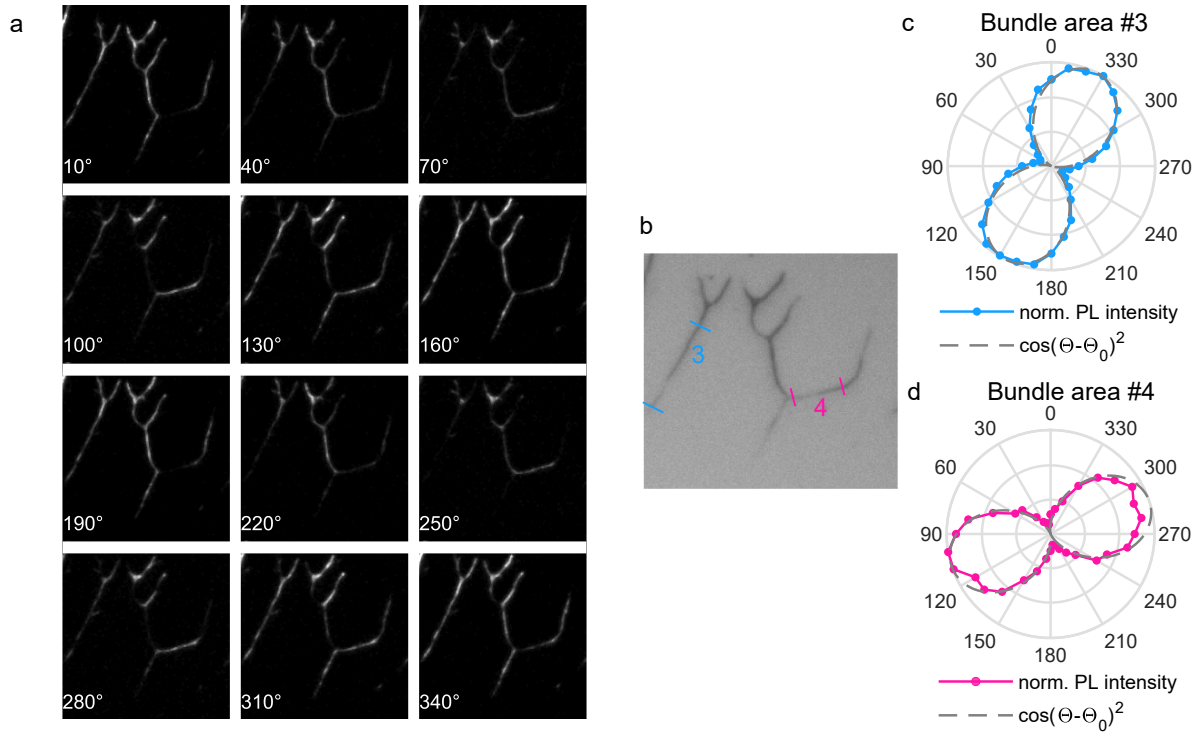

Figure S11: (a) Polarization PL image series for $CsPbBr_3$@BNNT tubes (DMF-washed) as on Figure 4, in the 430-490 nm emission range. (b) Bright light image of the same area. (c,d) Polar plots of the PL intensity as a function of analyzer angle. The scale is normalized to the intensity maximum. Marks in panel b indicate bundle sections, based on which the polar plots were created.

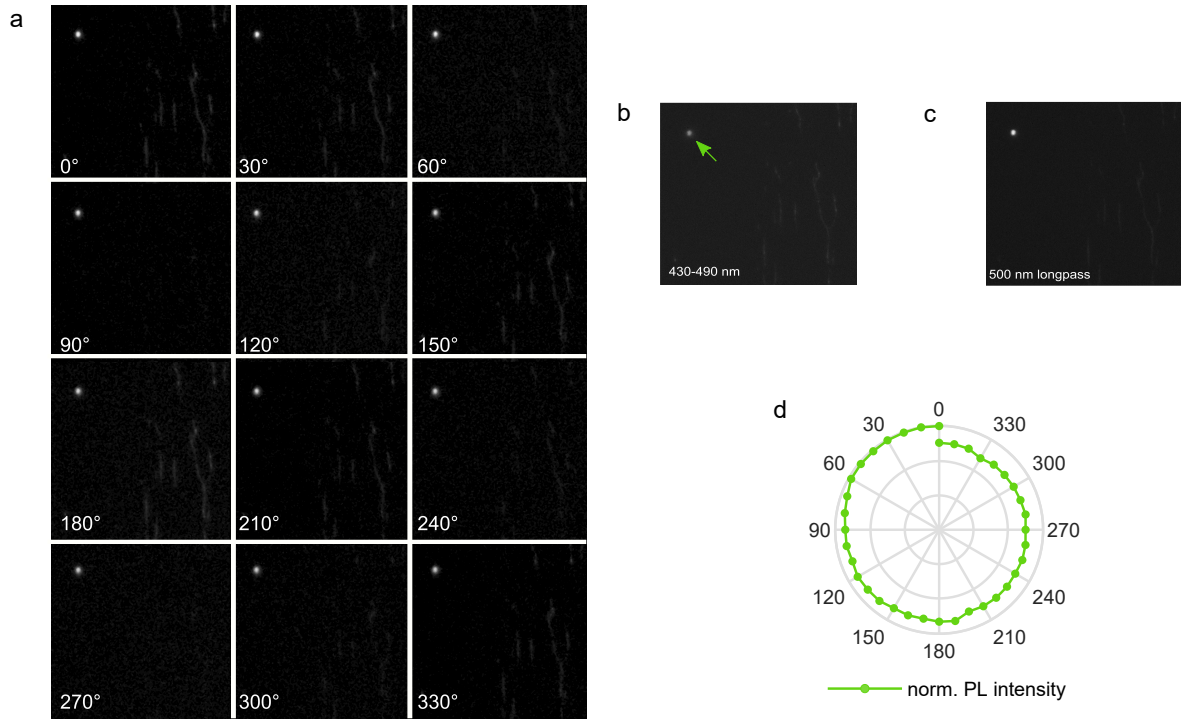

Figure S12: (a) Polarization PL image series for a non-encapsulated green emitter on a $CsPbBr_3$@BNNT sample. PL image using (b) a 430-490 nm bandpass filter and (c) 500 nm longpass filter. Arrow indicates the dot, whose (d) photoluminescence versus the analyzer angle is displayed in the polar plot. The scale is normalized to the intensity maximum.

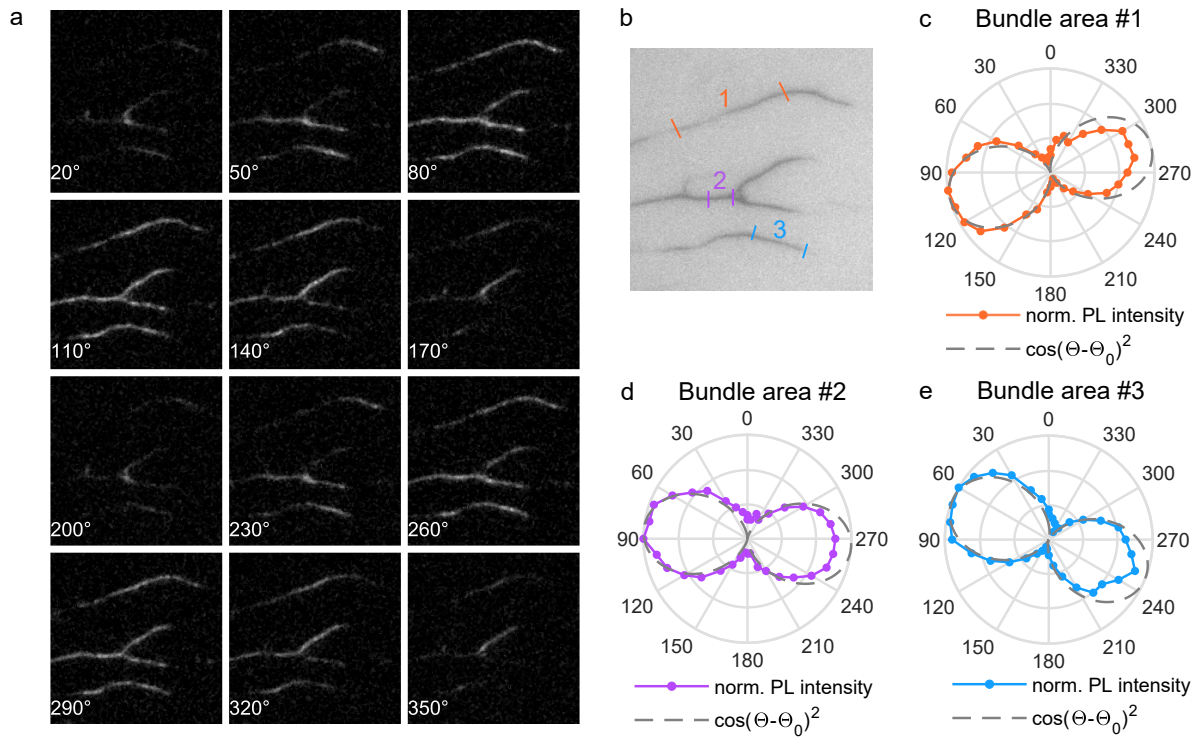

Figure S13: (a) Polarization PL image series for $CsPbI_3$@BNNT tubes. Images were recorded using a 550 nm longpass filter. (b) Bright light image of the same area. (c,d,e) Polar plots of the PL intensity as a function of analyzer angle. The scale is normalized to the intensity maximum. Marks in panel b indicate bundle sections, based on which the polar plots were created.

9 Reference for emission stability

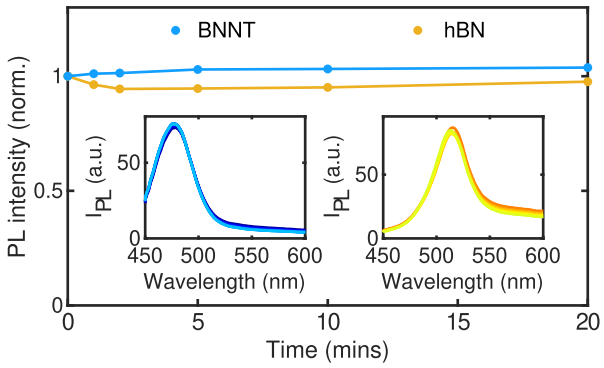

Figure S14: Photoluminescence intensity measured upon 20 minutes continuous illumination inside the glovebox on the unwashed $CsPbBr_3$@BNNT sample and a reference sample containing predominantly hBN embedded $CsPbBr_3$ nanoparticles (as described in section Reference for non-confined species, Fig. S5b and c. The graph is normalized to the intensity of the first measurement. Spectra were recorded using a 405 nm laser excitation at 5 mW by a laser pointer. Insets are showing the corresponding PL spectra.

References

(1) Straus, D. B.; Guo, S.; Cava, R. J. Kinetically Stable Single Crystals of Perovskite-Phase $CsPbI_3$. *Journal of the American Chemical Society* **2019**, *141*, 11435–11439.

(2) Hadjiev, V. G.; Wang, C.; Wang, Y.; Su, X.; Calderon, H. A.; Robles Hernandez, F.; Wang, Z. M.; Bao, J. M. Phonon Fingerprints of $CsPb_2$ Br_5. *Journal of Physics: Condensed Matter* **2018**, *30*, 405703.

(3) Fang, X.; Zhang, K.; Li, Y.; Yao, L.; Zhang, Y.; Wang, Y.; Zhai, W.; Tao, L.; Du, H.; Ran, G. Effect of Excess $PbBr_2$ on Photoluminescence Spectra of $CH_3NH_3PbBr_3$ Perovskite Particles at Room Temperature. *Applied Physics Letters* **2016**, *108*, 071109.

(4) Lee, S. M.; Moon, C. J.; Lim, H.; Lee, Y.; Choi, M. Y.; Bang, J. Temperature-Dependent Photoluminescence of Cesium Lead Halide Perovskite Quantum Dots: Splitting of the

Photoluminescence Peaks of $CsPbBr_3$ and $CsPb(Br/I)_3$ Quantum Dots at Low Temperature. *The Journal of Physical Chemistry C* **2017**, *121*, 26054–26062.

(5) Walker, K. E.; Rance, G. A.; Pekker, Á.; Tóháti, H. M.; Fay, M. W.; Lodge, R. W.; Stoppiello, C. T.; Kamarás, K.; Khlobystov, A. N. Growth of Carbon Nanotubes inside Boron Nitride Nanotubes by Coalescence of Fullerenes: Toward the World's Smallest Coaxial Cable. *Small Methods* **2017**, *1*, 1700184.

(6) Tutantsev, A. S.; Udalova, N. N.; Fateev, S. A.; Petrov, A. A.; Chengyuan, W.; Maksimov, E. G.; Goodilin, E. A.; Tarasov, A. B. New Pigeonholing Approach for Selection of Solvents Relevant to Lead Halide Perovskite Processing. *The Journal of Physical Chemistry C* **2020**, *124*, 11117–11123.

(7) Cheng, S.; Zhong, H. What Happens When Halide Perovskites Meet with Water? *The Journal of Physical Chemistry Letters* **2022**, *13*, 2281–2290.

(8) Özeren, M. D.; Pekker, Á.; Kamarás, K.; Botka, B. Evaluation of Surface Passivating Solvents for Single and Mixed Halide Perovskites. *RSC Advances* **2022**, *12*, 28853–28861.

(9) Liang, T.; Liu, W.; Liu, X.; Li, Y.; Wu, W.; Fan, J. *In Situ* Phase-Transition Crystallization of All-Inorganic Water-Resistant Exciton-Radiative Heteroepitaxial $CsPbBr_3$ –$CsPb_2$ Br_5 Core–Shell Perovskite Nanocrystals. *Chemistry of Materials* **2021**, *33*, 4948–4959.

(10) Cheng, O. H.-C.; Qiao, T.; Sheldon, M.; Son, D. H. Size- and Temperature-Dependent Photoluminescence Spectra of Strongly Confined $CsPbBr_3$ Quantum Dots. *Nanoscale* **2020**, *12*, 13113–13118.

(11) Zhu, M.; Yin, H.; Cao, J.; Xu, L.; Lu, P.; Liu, Y.; Ding, L.; Fan, C.; Liu, H.; Zhang, Y.; Jin, Y.; Peng, L.-M.; Jin, C.; Zhang, Z. Inner Doping of Carbon Nanotubes with Perovskites for Ultralow Power Transistors. *Advanced Materials* **2024**, *36*, 2403743.

(12) Hatting, B.; Heeg, S.; Ataka, K.; Heberle, J.; Hennrich, F.; Kappes, M. M.; Krupke, R.; Reich, S. Fermi Energy Shift in Deposited Metallic Nanotubes: A Raman Scattering Study. *Physical Review B* **2013**, *87*, 165442.

(13) Wang, K.; Zhao, Y.; Geng, L.; Wang, H.; Teng, Y.; Yao, J.; Zhou, C.; Li, X.; Zhao, P.; Wang, Y.; Liang, H.; Zhang, Y.; Tian, D.; Kang, L. Editable Light Response in Halide Perovskites Encapsulated within Single-Walled Carbon Nanotubes. *ACS Nano* **2025**, *19*, 16110–16118.